IOP Publishing New J. Phys. 22 (2020) 013007 https://doi.org/10.1088/1367-2630/ab623b

New Journal of Physics
The open access journal at the forefront of physics

Deutsche Physikalische Gesellschaft DPG
IOP Institute of Physics

Published in partnership with: Deutsche Physikalische Gesellschaft and the Institute of Physics

OPEN ACCESS

RECEIVED
8 August 2019

REVISED
13 November 2019

ACCEPTED FOR PUBLICATION
16 December 2019

PUBLISHED
14 January 2020

PAPER

Spin-dependent radiative deflection in the quantum radiation-reaction regime

X S Geng[1,2], L L Ji[1,3,5], B F Shen[1,3,4,5], B Feng[1,2], Z Guo[1,2], Q Q Han[1,2], C Y Qin[1,2], N W Wang[1], W Q Wang[1,2], Y T Wu[1,2], X Yan[1,2], Q Yu[1,2], L G Zhang[1] and Z Z Xu[1]

[1] State Key Laboratory of High Field Laser Physics, Shanghai Institute of Optics and Fine Mechanics, Chinese Academy of Sciences, Shanghai 201800, People's Republic of China
[2] University of Chinese Academy of Sciences, Beijing 100049, People's Republic of China
[3] Center for Excellence in Ultra-intense Laser Science, Chinese Academy of Sciences Shanghai 201800, People's Republic of China
[4] Shanghai Normal University, Shanghai 200234, People's Republic of China
[5] Author to whom any correspondence should be addressed.

E-mail: jill@siom.ac.cn and bfshen@mail.shcnc.ac.cn

Keywords: spin, ultra-intense laser, strong-field QED, radiation reaction

Abstract

A new spin-dependent deflection mechanism is revealed by considering the spin-correlated radiation-reaction force during laser-electron collision. We found that such deflection originates from the non-zero work done by the radiation-reaction force along the laser polarization direction in each half-period, which is larger/smaller for spin-anti-paralleled/spin-paralleled electrons. The resulted anti-symmetric deflection is further accumulated when the spin-projection onto the laser magnetic field is reversed in adjacent half-periods. The discovered mechanism dominates over the Stern–Gerlach deflection for electrons of several hundreds of MeV and 10 PW-level laser peak power. The results provide a new perspective to study the strong-field QED physics in quantum radiation-reaction regime and an approach to leverage the study of radiation-dominated and strong-field QED physics via particle spins.

1. Introduction

Spin is an intrinsic property of particles that can play a role in the motion of a moving particle, as illustrated by the famous Stern–Gerlach (SG) experiment [1]. A particle with non-zero spin can be deflected by SG effect in the inhomogeneous magnetic field. In general, the spin effect strongly depends on the gradient of the magnetic field. Optical lasers, with light intensities approaching 10^{23} W cm^{-2}, provide large gradient of magnetic fields at the order of 10^6 T within a few microns. Therefore it is a promising driver to trigger the spin effect on particle dynamics. Previous studies have shown that by colliding $\sim 10^1$ MeV electrons with a laser of $\sim 10^{22}$ W cm^{-2}, electrons with spin up/ down can be deflected to an angle of $\pm 10^{-7}$ rad by the SG force [2]. In the regime where SG effect emerges during collision, it is expected that other exotic phenomena become significant. For instance, electrons emit high-energy gamma-photons via non-linear Compton scattering and consequently feel recoil, which is usually referred to as radiation-reaction (RR) force [3, 4]. In the case where the photon energy is comparable to the electron energy, quantum behavior appears such that the radiation turns to be stochastic [5–10]. The electron motion therefore is governed by the quantum radiation-reaction effect in the strong field quantum electro-dynamics (QED) picture.

In the QED perspective, when the spin state of an electron is considered it has been found out that the spin-anti-paralleled electron tends to radiate more energy than the spin-paralleled electron and that the electron may undergo a spin-flip process during photon emission [11, 12]. Spin-flip effect along with the so-called 'quantum-jump' process were also proposed to polarize an electron beam in collision with an elliptically polarized laser pulse [13]. However, in a linearly-polarized (LP) laser pulse the electron spin projection onto the magnetic field axis in its rest frame oscillates with the laser field and the spin-induced net contribution is averaged to zero. Considering the SG effect being too weak as compared to the RR effect [2], present scenarios thus predict no sign of significant spin-dependent dynamics for LP laser fields with symmetric field distribution, except that asymmetry is introduced to the field itself in the few-cycle regime [12, 13]. The new mechanism results from the coupling between the strong radiation reaction and spin effect, which is not active in the parameters investigated in [12]

In this work, we show a new mechanism that leads to significant deflection of electrons by spin-induced effect in a symmetric LP laser field. This is only possible by coupling the spin dynamics into the radiation-reaction force. The mechanism, which has not been revealed before, does not rely on artificially introduced asymmetry of the field but on the intrinsic oscillating nature of the laser field. We examined the spin-dependent radiation via the classical and the QED model, which both gave consistent results. This distinctive spin-dependent effect dominates the SG deflection effect under the configuration considered in the current work and accessible for the next-generation 10–100 PW laser facilities [14–19].

This paper is organized as follows: in section 2, we introduce both the classical and quantum models of spin-dependent radiation-reaction; in section 3, the deflection of polarized electron by spin-dependent radiation and its mechanism are presented; in section 4, the spin-dependent scenario is reproduced in the unpolarized electron beam by sign of asymmetric distribution of the polarization of the scattered electrons.

2. Theoretical and numerical methods

2.1. QED Spin-dependent radiation-reaction model

To model the stochastic photon emission, we employ the Monte-Carlo (MC) algorithm. The electron motion as well as the spin dynamics between photon emission events are treated classically and the photon emission probability is based on QED calculations. Electron motion and spin dynamics follow the Lorentz equation $\mathrm{d}\mathbf{p}/\mathrm{d}t = -e(\mathbf{E} + \mathbf{p} \times \mathbf{B}/\gamma m)$ and the Thomas–Bargmann–Michel–Telegdi equation [20]

$$\frac{\mathrm{d}\mathbf{s}}{\mathrm{d}t} = \frac{e}{mc}\mathbf{s} \times \left[\left(\frac{g_e}{2} - 1 + \frac{1}{\gamma}\right)\mathbf{B} - \left(\frac{g_e}{2} - 1\right)\frac{\gamma}{\gamma + 1}(\boldsymbol{\beta} \cdot \mathbf{B})\boldsymbol{\beta} - \left(\frac{g_e}{2} - \frac{\gamma}{\gamma + 1}\right)\boldsymbol{\beta} \times \mathbf{E}\right], \tag{1}$$

where $\mathbf{E}$ and $\mathbf{B}$ are the electric and magnetic fields, $\mathbf{p}$ the momentum, γ the Lorentz factor, e the electron charge, m the electron mass and $a_e = \frac{g_e - 2}{2} \approx 1.16 \times 10^{-3}$ the anomalous magnetic moment of electron [21]. The QED-based photon emission process including electron spin is correlated to the radiation spectrum of the electron for the spin-paralleled/-anti-paralleled case, similar to the Sokolov–Ternov effect [11] (see also [22]) under the locally constant field approximation (LCFA):

$$\begin{aligned} F(y) = \frac{9\sqrt{3}}{16\pi(1 + \xi y)^4}\Bigg(&\frac{1 + \zeta\zeta'}{2}\left\{\left(1 + \frac{\xi y}{2}\right)^2\left[\int_y^\infty K_{5/3}(x)\mathrm{d}x + \rho K_{2/3}(y)\right]\right.\\ &\left. + \left[\frac{\xi^2 y^2}{2}\int_y^\infty K_{1/3}(x)\mathrm{d}x - \zeta'(2 + \xi y)\xi y K_{1/3}(x)\right]\frac{1 + \rho}{2}\right\}\\ &+ \frac{1 - \zeta\zeta'}{2}\frac{\xi^2 y^2}{4}\left\{\int_y^\infty K_{5/3}(x)\mathrm{d}x - \rho K_{2/3}(y)\right.\\ &\left. + \left[2\int_y^\infty K_{1/3}(x)\mathrm{d}x - 4\zeta' K_{1/3}(y)\right]\frac{1 - \rho}{2}\right\}\Bigg), \end{aligned} \tag{2}$$

where $F(y)$ is the synchrotron function, $\zeta\zeta'$ the initial/final quantization value of spin, ρ the photon polarization, $\xi = 3\chi_e/2$, $\chi_e = e\hbar|F \cdot p|/m^3c^4$, $y = \frac{2}{3}\chi_e^{-1}\frac{\delta}{1 - \delta}$, $\delta = \hbar k \cdot \hbar k'/\hbar k \cdot p$ the photon energy fraction. The theory for arbitrarily polarized electrons is further developed by D Seipt *et al* in [12]. For electron polarization vector of $\mathbf{s}$ in its rest frame, the radiation probability rate is [12]

$$\mathbb{P}^{s,\chi}(\delta) = \frac{\mathrm{d}P}{\mathrm{d}\delta\mathrm{d}\psi} = -\frac{\alpha}{b}\left[\mathrm{Ai}_1(z) + g\frac{2\mathrm{Ai}'(z)}{z} + s_\zeta\delta\frac{\mathrm{Ai}(z)}{\sqrt{z}}\right], \tag{3}$$

where α is the fine structure constant, $b = \hbar k \cdot p/m^2c^2$, Ai($z$) the Airy function, ψ the laser phase, $\hbar k$, $\hbar k'$ and p the four-momentum of laser, photon and electron, $z = \left[\frac{\delta}{(1 - \delta)\chi_e}\right]^{2/3}$, $g = 1 + \delta^2/[2(1 - \delta)]$, F the electromagnetic tensor, e the electron charge, $\hbar$ the reduced Planck constant, m the electron mass at rest, c the speed of light and $s_\zeta = \mathbf{s} \cdot \hat{\mathbf{B}}_{\mathrm{rest}}$, respectively. Here $\hat{\mathbf{B}}_{\mathrm{rest}}$ is the direction of the magnetic field in the electron's rest frame. The results by D Seipt *et al* are based on the LCFA. This approximation is usually applied when the formation length of 'synchrotron-like' radiation is much smaller as compared to the featured scale of the driving field. In the case of laser-electron interaction, it has been shown that LCFA is valid at $a_0^3/\chi_e \gg 1$ [23] and the radiation of low energy photon is valid for $\delta \gg \chi_e/a_0^3$ [24]. In this work, we have $a > 100$ and $\chi_e < 1$, well beyond the above criteria. Here, $a_0 = eE/mc\omega$ is the invariant field strength parameter.

The spin-dependent spectrum of an electron in (anti-)parallel state given by equation (3) is consistent the results from the well-known Sokolov–Ternov equation in equation (2). The radiation probability can also be classified to spin-flip case $\mathrm{d}P_{\mathrm{flip}}/\mathrm{d}\delta\mathrm{d}\psi$ and non-flip one $\mathrm{d}P_{\mathrm{nonflip}}/\mathrm{d}\delta\mathrm{d}\psi$ [12], for convenience of numerical modeling, where the electron undergoes $\mathbf{s} \rightarrow -\mathbf{s}$ during photon emission in the spin-flip case.

The QED-MC algorithm is implemented to calculate photon emission events. At each time step, the radiation probability rate $\mathbb{P}$ is calculated according to the local χ_e value as well as the spin state. According to the QED-MC methods in [25], two uniform random numbers are generated in the [0, 1] section to sample the spectrum of the probability rate. The probability rate calculated with the first random number r_1 is multiplied with time step $\Delta\psi$. If the second random number $r_2 < \mathbb{P} \cdot \Delta\psi$, then a photon of energy r_1 is radiated. Photon recoil $\Delta p = r_1 \cdot \gamma mc$ is applied to the electron via momentum conservation after photon emission. To solve the energy cut-off in the low energy part of the spectrum introduced by numerical methods, we implement the modified event generator [25] to include the low energy photon emission.

The spin-flip and non-flip events are calculated by the weights of the flip probability rate $\mathbb{P}_{\mathrm{flip}}/\mathbb{P}$ at each time step. If another uniformly generated random number $r_3 < \mathbb{P}_{\mathrm{flip}}/\mathbb{P}$, electron undergoes $\mathbf{s} \rightarrow -\mathbf{s}$ process; otherwise the spin stays undisturbed by radiation.

2.2. Classical spin-dependent radiation-reaction model

For classical description of spin-dependent radiation, one can multiply a Gaunt factor calculated by averaging equation (2) [26] to the classical Landau–Lifshitz equation [27]

$$g^s = [1 + 2.54(\chi_e^2 - 1.28s\chi_e) + (4.34 + 2.58s)(1 + \chi_e) \times \ln(1 + (1.98 + 0.11s)\chi_e)]^{-2/3}. \tag{4}$$

The electron spin is parallel or anti-parallel to the chosen axis $\mathbf{B}_{\mathrm{rest}}$. In ultra-relativistic limit, the RR force is approximately $\mathbf{F}_{\mathrm{RR}}^s \sim g^s a^2\gamma^2$. As we will show later, the results from the classical spin-dependent RR from equation (4) are consistent with the one from statistics of the QED calculation using equation (3). The contribution from spin-flip process is ignored here due to low flip-rate. The stochastic quantum effect is omitted in classical description. However, its averaged representation successfully interprets the spin-dependent radiative deflection. As a comparison, we also calculate the deflection from the Stern–Gerlach force $\mathbf{F}_{\mathrm{SG}} = q/m\boldsymbol{\nabla}(\mathbf{s} \cdot \mathbf{B}_{\mathrm{eff}})$ induced by the gradient of the field, where $\mathbf{B}_{\mathrm{eff}} = \mathbf{B}/\gamma - \mathbf{p} \times \mathbf{E}/\gamma mc^2/(\gamma + 1)$ [2].

3. Results

In our modeling, the laser propagates along the z-axis, with $\hat{\mathbf{x}}$ the E-field direction and $\hat{\mathbf{y}}$ the B-field direction. Electron spin is defined in this coordinate with a unit vector; e.g. (0, $\pm$ 1,0) indicates the spin is parallel/anti-parallel to the y-axis. Head-on collision between polarized electrons and a laser is firstly investigated using the QED-MC method. We start with the simplest situation where the laser is approximated by

$$\mathbf{E} = \hat{\mathbf{x}}E_0 \exp(-x^2/w_0^2)\sin(\psi/2N)^2\cos(\psi) \tag{5}$$

for the electric field and $\mathbf{B} = \hat{\mathbf{y}}E_x/c$ for the magnetic field. Here E_0 is the electric field amplitude, w_0 the beam waist at e^{-1}, $\psi = \omega t - kz$ the phase, N the pulse length measured by wavelength (800 nm), respectively. This is valid since the electrons pass only the near-axis part of the laser beam. Electrons are initially polarized along $\pm y$ so that the spin-vector does not precess. In the head-on collision setup and the approximation of (5), the $\hat{\mathbf{B}}_{\mathrm{rest}}$ is consistent with the magnetic field the laboratory frame because

$$\mathbf{B}_{\mathrm{rest}} = \gamma\mathbf{B} - \frac{\mathbf{p}}{mc^2} \times \mathbf{E} - \frac{(\mathbf{p} \cdot \mathbf{B})\mathbf{p}}{(\gamma + 1)mc^2} = \hat{\mathbf{y}}(\gamma - \sqrt{\gamma^2 - 1}\beta_z)B_{\mathrm{lab}}(\psi, \mathbf{r}), \tag{6}$$

where $\beta = \mathbf{v}/c$. Therefore $\mathbf{s} \cdot \hat{\mathbf{B}}_{\mathrm{rest}}$ oscillates with laser phase.

In QED-MC modeling, we find that there is no tendency of anti-symmetric deflection for a spin-free electron, i.e. the averaged deflection angle $\langle\theta\rangle$ stays near zero. However, when spin is considered, electrons of opposite spin-orientation ($\pm$) tend to be scattered to opposite directions (figure 1(a)) via QED-MC. One finds more electrons of parallel/anti-parallel polarization in the upper ($\theta > 0$) / lower ($\theta < 0$) region, resulting in slight asymmetry of electron distribution along θ in figure 1(b). We qualify such asymmetric distribution by defining the averaged deflection angle $\langle\theta\rangle$. The phenomenon is investigated in a large parameter regime as shown in figures 1(b)–(e). We focus on the $\chi_e < 1$ region, e.g. Figure 1(b) where pair-production [28] is suppressed [29]. The averaged deflection angle is calculated by repeating the collision for sufficient number of times (10^6 times in figure 1(b) and and 10^5 times in figures 1(c)–(e)) under each set of parameters. For fixed electron energy, larger field strength can separate electrons of different initial spin-orientation to larger angles, as shown in figure 1(b), while the deflection angle of spin-free electrons stays near zero as $\gamma_0 \gg a_0$. The deflection angle is slightly reduced when spin-flip is turned on. Since every electron flips only 0.18 time in average at $a_0 = 150$, $\gamma_0 = 1000$ according to our modeling, the modification is so minor as shown in figure 1(b) that we

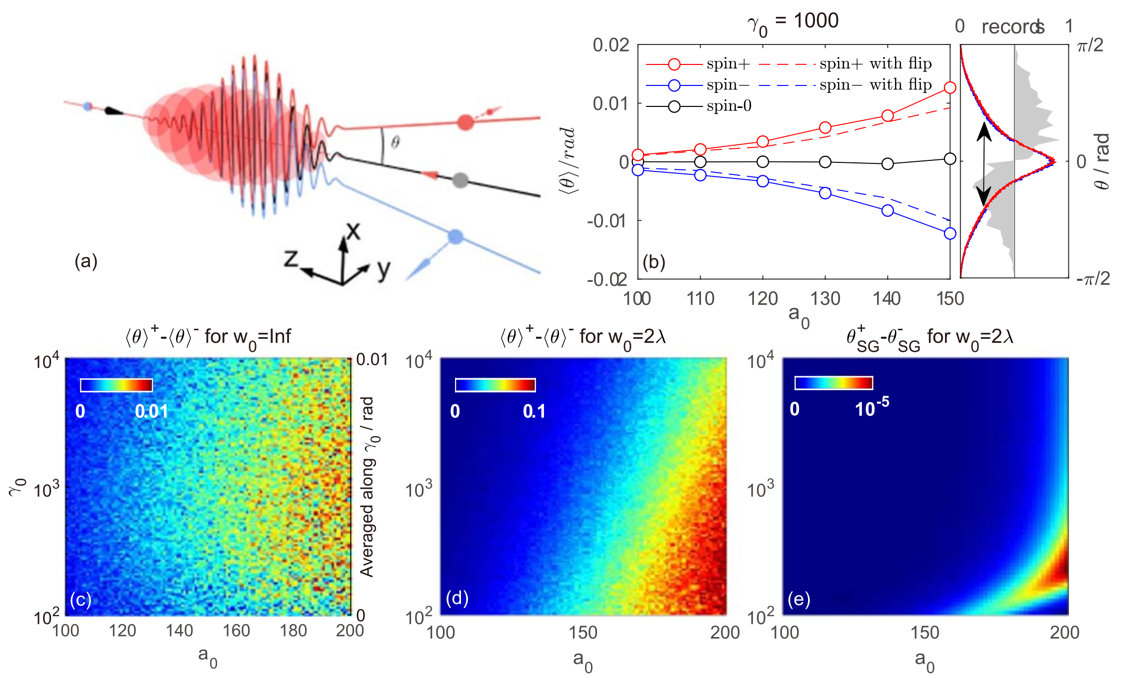

Figure 1. (a) Collision between a polarized electron and a strong laser pulse. The electron propagates along $-z$ direction; the laser propagates along z direction with polarization along x. Electrons of different initial spin polarization, i.e. parallel (red)/anti-parallel (blue), get deflected to opposite direction due to spin-dependent radiation-reaction while the spin-free electron (gray) stays undeflected. (b) The deflection angle for different field strength with $\gamma_0 = 1000$. Curves on the right are the angular distribution of $\pm$ polarized electrons after collision for $a_0 = 150$, $T_{\mathrm{FWHM}} = 27$ fs and $w_0 = 2\lambda$; the gray area is the difference between spin $\pm$. Electron records are normalized in all cases. (c)–(e) Averaged deflection angle between spin $\pm$ electrons without transverse ponderomotive scattering ((c), $w_0 = \mathrm{Inf}$), with ponderomotive scattering ((d), $w_0 = 2\lambda$) and for the Stern–Gerlach deflection (e) in the $a_0 - \gamma_0$ parametric space.

will not include it in the following. We note that the spread of the scattered angle in figure 1(b) is a clear reflection of the stochastic nature of QED photon emission.

It should be noted that when the beam waist is not included (no transverse ponderomotive scattering), as illustrated in figure 1(c), the deflection angle scales linearly with a_0 and weakly depends on γ_0. The deflection angle peaks in the area of higher a_0 and smaller γ_0 when there is a finite laser beam waist, as shown in 1(d). By comparing figure 1(c) to 1(d) one sees the amplification of the electron deflection induced by the transverse laser ponderomotive force. The latter is more effective for lower electron energies and stronger laser fields. The SG force can also deflect electrons in a similar way, but at a much smaller level (10^{-5} rad) as shown in figure 1(e).

We now focus on the ponderomotive oscillation of an electron during its collision with a plane-wave as shown in figure 2(a). When RR force is included, since $\mathbf{F}_{\mathrm{RR}} \sim \gamma^2$ the electron loses its energy during oscillation such that the work done by RR force towards x-direction cannot be fully compensated by the one along the $-x$-direction, i.e. $\left|\int_{\mathrm{rise}} \mathrm{d}\psi \mathbf{F}_{\mathrm{RR}} \cdot \hat{\mathbf{x}}\right| > \left|\int_{\mathrm{fall}} \mathrm{d}\psi \mathbf{F}_{\mathrm{RR}} \cdot \hat{\mathbf{x}}\right|$. Consequently the net work is non-zero in the half-period. As seen in figure 2(a), in each half-period of the trajectory the damping force induces net negative/positive momentum shift Δp_x^{RR} (Δp_x is used for convenience) for the concave-down/-up curve, denoted by down/up black arrows in figure 2(a). For a spin-free electron, the momentum shifts in adjacent half-periods are nearly equal in amplitude, exhibiting near-zero deflection effect.

This symmetry is broken when spin is coupled to the RR force. One can find in equation (3) or in equation (4) that electrons radiate more energies when anti-paralleled to $\mathbf{B}_{\mathrm{rest}}$. As a result, an electron experiences larger (anti-parallel) or smaller (parallel) $\mathbf{F}_{\mathrm{RR}}$ compared to a spin-free electron. Take the electron with spin parallel to $\mathbf{B}_{\mathrm{rest}}$ ($\mathbf{B}_{\mathrm{lab}}$ equivalently) as an example, in the first half-period the momentum shift Δp_x^+ (+ denotes initially paralleled spin) along the negative $\mathbf{s} \times \mathbf{k}$ direction is smaller compared to the spin-free case, as shown by the shorter red arrow in figure 2(a). However, in the next half-period, the laser magnetic field is flipped while the spin orientation remains unchanged. The spin state is switched from parallel to anti-parallel to $\mathbf{B}_{\mathrm{rest}}$. According to equation (4), the higher radiation power for anti-parallel spin corresponds to a larger momentum shift, only that it is directed along the positive $\mathbf{s} \times \mathbf{k}$ axis, as shown by the longer red arrow in figure 2(a). By integrating the momentum change along the x-direction, one finds a net shift relative to the spin-free electron in the $\mathbf{s} \times \mathbf{k}$ direction. For electron of anti-paralleled initial spin, the process is similar but the net momentum shift is flipped due to the opposite $\mathbf{s} \times \mathbf{k}$ vector.

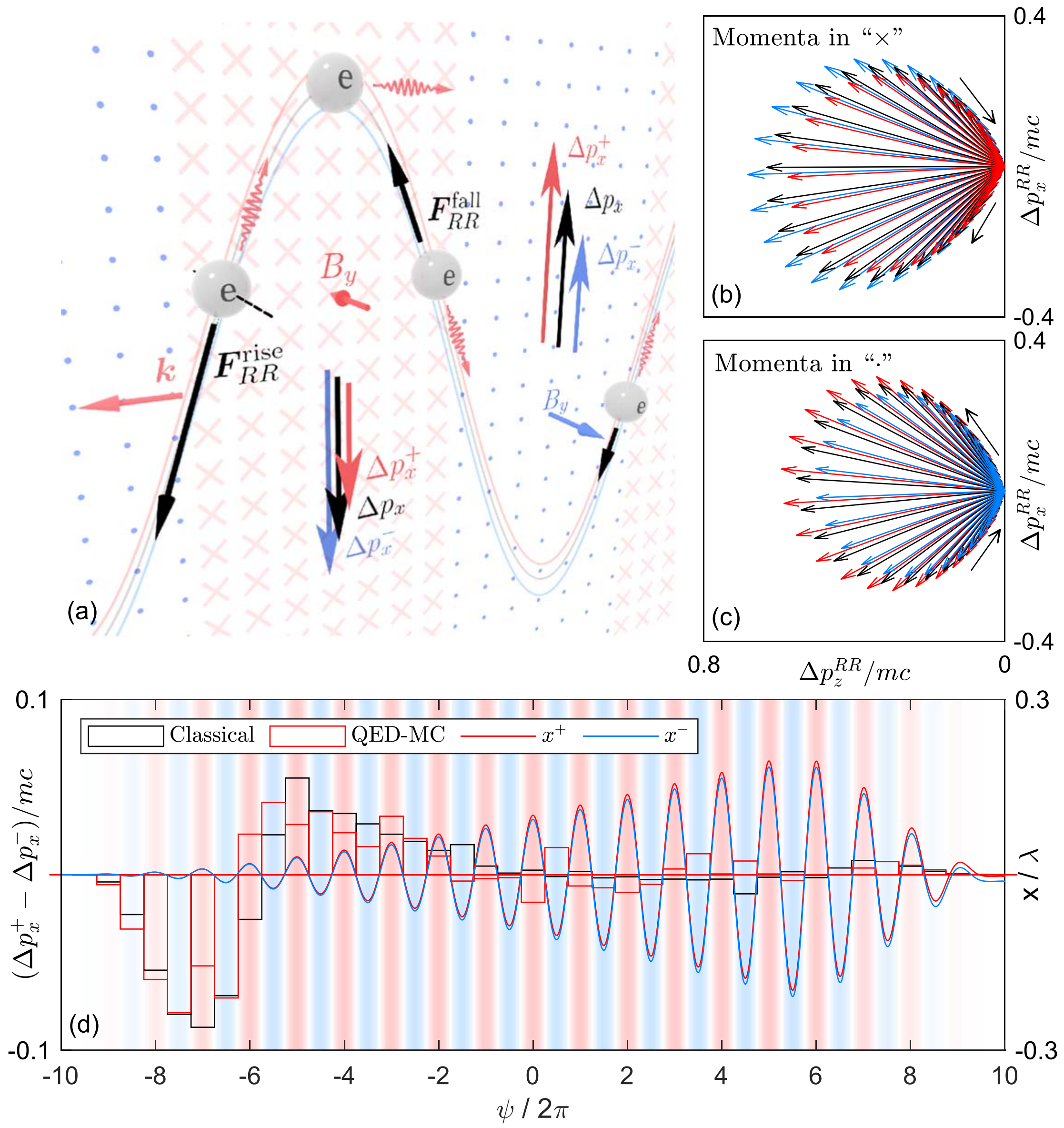

Figure 2. An electron collides with a flat-top laser pulse where the plateau region is $-5 < \psi/2\pi < 5$ for spin +/− (red/blue) and spin-free (black). (a) Electron trajectories (curves) and momentum change due to RR in x-direction in half-period (Δp_x and arrows). The lengths of arrows indicate the length of the vector. (b)–(c) The variation of vector Δp^{RR} along the collision time steps for adjacent half-periods ('×' for (b), '·' for (c)). Integrate the vectors along x and one will get $\Delta p_x^{\pm}$ shown in (a). (d) The electron trajectories of initially +/− polarized electron (red/blue lines) and the difference between $\Delta p_x^{\pm}$ accumulated in half-periods for classical radiation (black bars) and QED-MC radiation (red bars).

The analysis is validated from the momentum shift Δp_x^{RR} at each time step in figures 2(b)–(c), where $|\Delta p_x^+| < |\Delta p_x| < |\Delta p_x^-|$ in the first half-period and $|\Delta p_x^+| > |\Delta p_x| > |\Delta p_x^-|$ in the next. The electron always experiences a net momentum shift towards the $\mathbf{s} \times \mathbf{k}$ axis relative to the spin-free electron. This imbalance is accumulated in many oscillating periods and eventually builds up a significant deflection.

The accumulation of the spin-dependent deflection is clearly seen in figure 2(d) where we collide electrons of $\gamma_0 = 1000$ with flat-top plane-wave pulse. We focus on the plateau ($-5 < \psi/2\pi < 5$) to exclude the effect of the rising/falling edge. Here the classical equation of motion with spin-dependent Gaunt factor is employed so that the time-resolved dynamics are not influenced by stochastic effects from QED-MC. The difference between $\Delta p_x^{\pm}$ in each half-period is presented (black and red bars). One can see Δp_x^+ becomes greater than Δp_x^- after the plateau begins ($\psi/2\pi > -5$) and the electron trajectories gradually diverge, with one shifted upwards/downwards respect to the other. The deflection direction is determined by the $\mathbf{s} \times \mathbf{k}$ axis, which is exactly as predicted with our model in figure 2(a). Good consistency is seen in the QED-MC modeling from figure 2(d). The slight discrepancy between the QED and classical modeling arises from the stochastic trajectories of QED that strongly diverge for $\psi/2\pi > 0$. However, the classical trajectory can well reflect the momentum change of the QED trajectories in the $\psi/2\pi < 0$ section where the QED trajectories still cluster by the classical one.

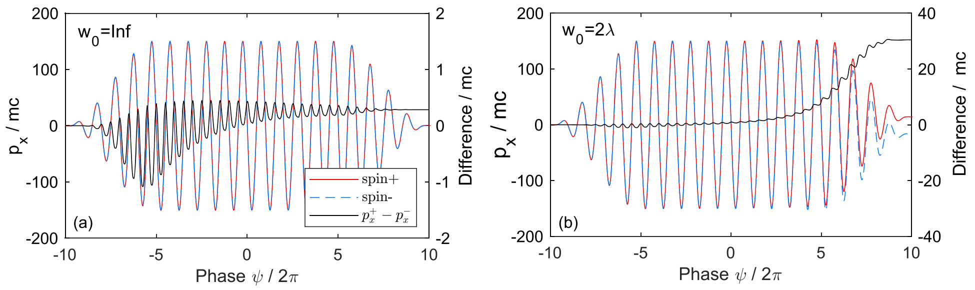

Figure 3. The momentum change of $\pm$ polarized electrons (red/blue line) during collision with a flat-top laser with $w_0 = 2\lambda$ (a) and infinite beam waist (b). The difference between $p_x^{\pm}$ is shown by the black lines.

We note that in the rising edge of the pulse ($-10 < \psi/2\pi < -5$), the momentum change from RR is inversed, i.e. $\Delta p_x^+ < \Delta p_x^-$, as shown by the negative black bars. In this case, the increase of the field strength in the rising edge dominates over the correction from spin-dependent radiation in terms of the RR force, therefore $\mathbf{F}_{\mathrm{RR}}^{\mathrm{fall}}$ overrides $\mathbf{F}_{\mathrm{RR}}^{\mathrm{rise}}$. The net work in x-direction is therefore opposite to that in the plateau region, $\left|\int_{\mathrm{fall}} \mathrm{d}\psi \mathbf{F}_{\mathrm{RR}} \cdot \hat{\mathbf{x}}\right| > \left|\int_{\mathrm{rise}} \mathrm{d}\psi \mathbf{F}_{\mathrm{RR}} \cdot \hat{\mathbf{x}}\right|$. Accordingly, in the falling edge we have $\Delta p_x^+ > \Delta p_x^-$ again. The counter-play between the field strength variation and the damping of γ can be clearly seen from $\mathbf{F}_{\mathrm{RR}} \sim a^2\gamma^2$.

For further analysis of the ponderomotive effect, the electron momentum is presented in figure 3 by colliding the electron with a flat-top laser of infinite beam waist and beam waist $w_0 = 2\lambda$. In figure 3, one can see that p_x oscillates with constant amplitude during the plateau while the difference between $+$(red) and $-$(blue) polarized electrons gradually builds up (black). The momentum discrepancy (the black-solid) directly proves the deflection by spin-dependent radiation. Such difference grows much quicker with the help of ponderomotive force ($\mathbf{F}_{\mathrm{pond}} \sim -\boldsymbol{\nabla}\mathbf{E}^2$) by comparing figure 3(a) to 3(b). We find that when the spin $\pm$ electrons are separated by the spin-dependent RR force the ponderomotive force will further increase the electrons' spacing δx. The difference of ponderomotive forces between spin $\pm$ electrons is $\delta F_{\mathrm{pond}}^x = \partial F_{\mathrm{pond}}^x/\partial x \cdot \delta x$, which is always positive for $|x| < w_0/2$ as

$$\frac{\partial}{\partial x} F_{\mathrm{pond}}^x \sim \frac{4}{w_0^2}\left(1 - \frac{4x^2}{w_0^2}\right)\exp\left(-\frac{2x^2}{w_0^2}\right).$$

Therefore $\delta F_{\mathrm{pond}}^x$ is further increased by the spacing δx. As a result, a positive feedback between ponderomotive effect and spin-dependent RR is built up.

4. Discussion

Now that the electron with opposite spin-orientation tend to be scattered to opposite directions in a collision with laser pulse, the averaged spin polarization therefore becomes inhomogeneous as a function of the scattered angle. We consider an unpolarized electron bunch of $\gamma_0 = 1000$ with transverse size of 4λ and 12λ at e^{-1} with energy spread of $\sim$1% and angular divergence of 10 mrad colliding with a laser pulse of $a_0 = 150$ via QED-MC, then the polarity of electrons is measured along y-direction ($\langle s_y \rangle$) for different scattering angle. The spin-flip process is omitted due to low flip-rate. We use a focused laser pulse [30] that expresses the components of the field to the fifth order of diffraction angle. The pulse length is 27 fs at FWHM and beam waist is 2λ at e^{-1}. In a focused pulse the spin precession needs to be considered. Spin-vector precession is calculated by solving the Thomas–Bargmann–Michel–Telegdi equation [20] . The electrons distribution stays symmetric along θ as shown in figure 4(b) while $\langle s_y \rangle$ is anti-symmetric alongas shown in figure 4(c). The bunch get polarized along y because the electrons with positive s_y tend to be scattered upwards while those with negative s_y downwards. Experimental measurement of this anti-symmetric phenomenon provides a new degree of freedom to study the quantum RR effect in addition to spin-free phenomena [7, 10, 31–33]. Effects of the electron beam energy spread and angular divergence are illustrated in figure 4(c). The mechanism is robust under realistic electron beam parameters. The deflection angle is dependent on the beam waist of the driving laser, which favors smaller focal spots, a natural consequence from the ponderomotive scattering. Considering that the polarization measurement at precession of the order 0.01 is demanding for polarimeters [34], one may also measure the asymmetric electron distribution for oppositely polarized electron beams as proposed in figure 1 to identify the new effect.

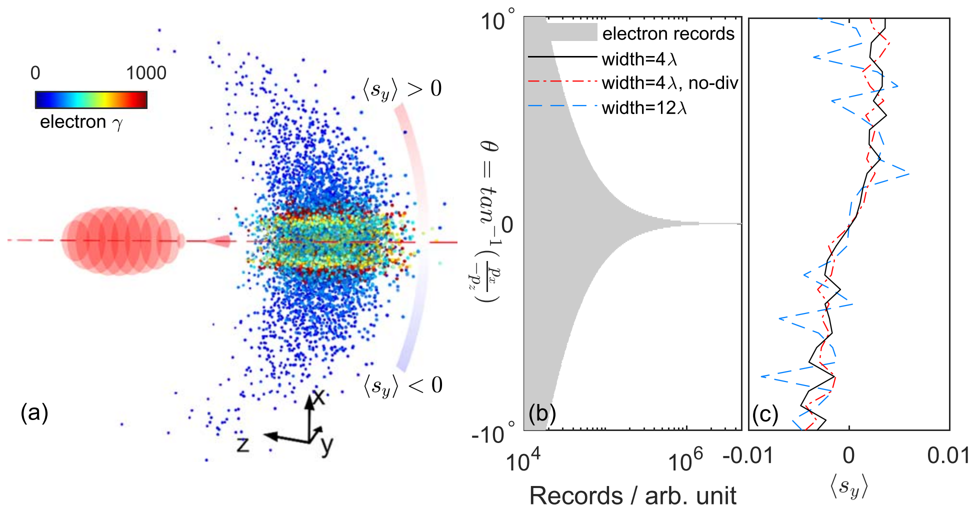

Figure 4. (a) Collision between a linearly polarized laser pulse of $a_0 = 150$ and an unpolarized electron bunch of $\gamma_0 = 1000$. The color of the electrons represents the energy of the electrons. The color bar on the right represents the spatial polarization along θ. The red/blue end represents positive/negative polarization. (b) Angular distribution after collision for electron transverse width of 4λ (gray area). (c) The angular distribution of the mean value of spin along y-axis for small transverse size of 4λ with 1% energy spread and 10 mrad angular divergence (black-solid), large transverse size of 12λ (blue-dashed) and transverse size of 4λ without energy and angular divergence (red-dotted–dashed).

5. Conclusion

In conclusion, we investigate the collision of initially polarized electron and laser pulse and find the deflection due to spin-dependent radiation-reaction. We successfully interpreted such deflection by studying the momentum losses during half-periods of phases for parallel and anti-parallel spin-state. It leads to non-vanishing anti-symmetric momentum shift during the collision which builds up the deflection gradually. The inhomogeneous polarity after collision is also observed for an unpolarized electron bunch. The new degree of freedom opens up the paths towards observing spin-dependent QED effects.

Acknowledgments

This work is supported by the Ministry of Science and Technology of the People's Republic of China (Grant Nos. 2018YFA0404803 and 2016YFA0401102), the National Science Foundation of China (Nos. 11875307 and 11935008), the Strategic Priority Research Program of Chinese Academy of Sciences (Grant No. XDB16010000) and the Recruitment Program for Young Professionals.

ORCID iDs

X S Geng https://orcid.org/0000-0003-1181-6518
L L Ji https://orcid.org/0000-0002-7107-0626
B F Shen https://orcid.org/0000-0003-1021-6991
Z Guo https://orcid.org/0000-0002-7827-9692

References

[1] Gerlach W and Stern O 1922 Der experimentelle nachweis der richtungsquantelung im magnetfeld *Z. Phys.* **9** 349–52
[2] Wen M, Keitel C H and Bauke H 2017 Spin-one-half particles in strong electromagnetic fields: spin effects and radiation reaction *Phys. Rev.* A **95** 042102
[3] Di Piazza A, Muller C, Hatsagortsyan K Z and Keitel C H 2012 Extremely high-intensity laser interactions with fundamental quantum systems *Rev. Mod. Phys.* **84** 1177–228
[4] Burton D A and Noble A 2014 Aspects of electromagnetic radiation reaction in strong fields *Contemp. Phys.* **55** 110–21
[5] Neitz N and Di Piazza A 2013 Stochasticity effects in quantum radiation reaction *Phys. Rev. Lett.* **111** 054802
[6] Vranic M, Grismayer T, Fonseca R A and Silva L O 2016 Quantum radiation reaction in head-on laser-electron beam interaction *New J. Phys.* **18** 073035
[7] Harvey C N, Gonoskov A, Ilderton A and Marklund M 2017 Quantum quenching of radiation losses in short laser pulses *Phys. Rev. Lett.* **118** 105004

[8] Li J X, Chen Y Y, Hatsagortsyan K Z and Keitel C H 2017 Angle-resolved stochastic photon emission in the quantum radiation-dominated regime *Sci. Rep.* **7** 11556
[9] Ridgers C P *et al* 2017 Signatures of quantum effects on radiation reaction in laser electron-beam collisions *J. Plasma Phys.* **83** 715830502
[10] Geng X S, Ji L L, Shen B F, Feng B, Guo Z, Yu Q, Zhang L G and Xu Z Z 2019 Quantum reflection above the classical radiation-reaction barrier in the quantum electro-dynamics regime *Commun. Phys.* **2** 66
[11] Ternov I M 1995 Synchrotron radiation *Phys.—Usp.* **38** 409
[12] Seipt D, Del Sorbo D, Ridgers C P and Thomas A G R 2018 Theory of radiative electron polarization in strong laser fields *Phys. Rev.* A **98** 023417
[13] Li Y-F, Shaisultanov R, Hatsagortsyan K Z, Wan F, Keitel C H and Li J-X 2019 Ultrarelativistic electron-beam polarization in single-shot interaction with an ultraintense laser pulse *Phys. Rev. Lett.* **122** 154801
[14] Shen B, Bu Z, Xu J, Xu T, Ji L, Li R and Xu Z 2018 Exploring vacuum birefringence based on a 100 pw laser and an x-ray free electron laser beam *Plasma Phys. Control. Fusion* **60** 044002
[15] Bashinov A V, Gonoskov A A, Kim A V, Mourou G and Sergeev A M 2014 New horizons for extreme light physics with mega-science project XCELS *Eur. Phys. J. Spec.Top.* **223** 1105–12
[16] Musgrave I *et al* 2013 Recent developments on the vulcan high power laser facility *SPIE Optics + Optoelectronics* vol 8780 (SPIE) p 14
[17] Le Garrec B *et al* 2017 Design update and recent results of the apollon 10 pw facility *SPIE Optics + Optoelectronics* vol 10238 (SPIE) p 6
[18] Mourou G and Tajima T 2011 The extreme light infrastructure: optics' next horizon *Opt. Photonics News* **22** 47–51
[19] Li R, Liang X, Leng Y and Xu Z 2017 Progress of the sulf 10 pw laser project *1st AAPPS-DPP Meeting*
[20] Jackson J D 1999 *Classical Electrodynamics* 3rd edn. (New York: Wiley)
[21] Schwinger J 1948 On quantum-electrodynamics and the magnetic moment of the electron *Phys. Rev.* **73** 416–7
[22] Del Sorbo D, Seipt D, Blackburn T G, Thomas A G R, Murphy C D, Kirk J G and Ridgers C P 2017 Spin polarization of electrons by ultraintense lasers *Phys. Rev.* A **96** 043407
[23] Podszus T and Di Piazza A 2019 High-energy behavior of strong-field QED in an intense plane wave *Phys. Rev.* D **99** 076004
[24] Di Piazza A, Tamburini M, Meuren S and Keitel C H 2018 Implementing nonlinear Compton scattering beyond the local-constant-field approximation *Phys. Rev.* A **98** 012134
[25] Gonoskov A, Bastrakov S, Efimenko E, Ilderton A, Marklund M, Meyerov I, Muraviev A, Sergeev A, Surmin I and Wallin E 2015 Extended particle-in-cell schemes for physics in ultrastrong laser fields: review and developments *Phys. Rev.* E **92** 023305
[26] Del Sorbo D, Seipt D, Thomas A G R and Ridgers C P 2018 Electron spin polarization in realistic trajectories around the magnetic node of two counter-propagating, circularly polarized, ultra-intense lasers *Plasma Phys. Control. Fusion* **60** 064003
[27] Landau L D and Lifshitz E M 1971 *The Classical Theory of Fields* (Oxford: Pergamon)
[28] Breit G and Wheeler J A 1934 Collision of two light quanta *Phys. Rev.* **46** 1087–91
[29] Ritus V I 1985 Quantum effects of the interaction of elementary particles with an intense electromagnetic field *J. Russ. Laser Res.* **6** 497–617
[30] Salamin Y I and Keitel C H 2002 Electron acceleration by a tightly focused laser beam *Phys. Rev. Lett.* **88** 095005
[31] Wistisen T N, Di Piazza A, Knudsen H V and Uggerhoj U I 2018 Experimental evidence of quantum radiation reaction in aligned crystals *Nat. Commun.* **9** 795
[32] Cole J M *et al* 2018 Experimental evidence of radiation reaction in the collision of a high-intensity laser pulse with a laser-Wakefield accelerated electron beam *Phys. Rev.* X **8** 011020
[33] Poder K *et al* 2018 Experimental signatures of the quantum nature of radiation reaction in the field of an ultraintense laser *Phys. Rev.* X **8** 031004
[34] Hauger M *et al* 2001 A high-precision polarimeter *Nucl. Instrum. Methods Phys. Res.* A **462** 382–92